# Heat Radiation Between Simply-Arranged Surfaces Having Different Temperatures and Emissivities

**E. M. SPARROW**

**University of Minnesota, Minneapolis, Minnesota**

**An analysis of radiant interchange is made which takes account of possible surface variations in incident radiation flux, heat transfer, and leaving radiant flux. This represents a generalization of standard calculation methods which postulate that the radiant fluxes and heat transfer are uniformly distributed on a surface. Consideration is given to pairs of simply-arranged surfaces having different emissivities, one of which is essentially black. The surface temperatures may be arbitrarily different. The generalized analysis reveals that there may be significant variations in the local heat transfer along a surface, and this stands in contrast to the results of standard (and more approximate) calculation methods. The over-all heat transfer results are also compared with those predicted by the standard calculation procedure. For the surface which is essentially black the errors arising in the standard procedure are found to be tolerable as long as the net over-all heat transfer exceeds 20% of the radiant emission. For the nonblack surface the two methods are in agreement.**

The recent revival of interest in radiation heat transfer owes its impetus to new technological developments. Attention is being given to more accurate and more detailed (local) analytical heat transfer predictions as well as to the radiation characteristics of complex configurations. Among other activities the standard procedures for calculating radiant exchange between surfaces are being re-evaluated and extended. Such a re-examination is the object of this paper; in addition results are presented for specific configurations.

Standard calculation methods for determining the radiant interchange between finite surfaces are presented in various heat transfer texts, (*1*, *2*). These methods are based on the postulates that each surface is isothermal and radiates and absorbs as a gray-body. It is additionally assumed that both emission and reflection are diffuse, that is that Lambert's cosine law is obeyed. The final assumption, which is perhaps somewhat less evident, arises from the use of angle factors between pairs of finite surfaces. The derivation of such angle factors contains the implicit assumption that the energy leaving a surface is uniformly distributed over that surface. However the energy leaving a surface is composed not only of direct emission but also of the reflection of the incident energy. Even if a surface is isothermal and emits uniformly over its area, it is highly unlikely that the incident energy will be uniformly distributed. Thus the assumption of uniform leaving flux is generally not satisfied.

The standard calculation method described above will be termed the "standard gray body enclosure theory." Its great utility arises from the fact that only linear algebraic equations need be dealt with. However a price must be paid for such simplicity. Only the over-all heat transferred from a surface can be calculated; the local heat transfer distribution along a surface cannot be determined. Also the over-all heat transfer results given by the standard theory are of uncertain accuracy because of the restrictive nature of the assumptions mentioned above.

Recent detailed analytical studies which evaluate and extend the standard gray body enclosure theory are reported in references 3 and *4*. In particular the restrictive assumption relating to the uniformity of the energy flux leaving a surface has been removed by reformulating the radiant interchange problem in terms of integral equations. Consideration was given to systems composed of simply-arranged surfaces having either equal or unequal temperatures but with equal emissivities. It was found that large variations in local heat flux could exist along a surface. But, in spite of this, the over-all heat transfer as predicted by the standard enclosure theory compared quite favorably with that from the more detailed analysis, and serious errors were sustained only for low emissivities and closely-spaced geometries. Additionally it was shown that the predictions of the standard theory were more accurate for radiation between surfaces having widely different temperatures than for surfaces having similar temperatures. There still remains to be explored the problem of radiant interchange between surfaces of highly different emissivities and, in particular, to obtain some measure of the accuracy of the standard enclosure theory for such a situation. It is this problem which is the subject of this paper. As in references *3* and *4* the author's concern here will be centered on the effects of the surface variation of the radiant flux.*

Specific consideration will be given to the three simple systems pictured in Figures 1(a), 1(b), and 1(c). The configurations, chosen because their simplicity will facilitate interpretation of the results, have been previously studied in references *3* and *4* but under the condition that the surface emissivities are equal. Thus the present analysis represents a logical extension of prior work.

Figure 1(a) represents a pair of parallel plates, each of length $L$ and separated by a distance $h$. The third dimension (into the plane of the page) is essentially infinite. The condition of highly unequal emissivities will be simulated by taking the upper surface (plate 1) as a black body $\epsilon = 1$, while the lower surface may have any other gray body emissivity. The temperatures $T_1$ and $T_2$ are uniform over their respective surfaces but may be arbitrarily different. The plates exchange heat with each other, and energy passes outward from between the plates to the external environment. For simplicity the external environment is assumed to be nonradiating. However because of the linearity of the problem any external radiation can always be added in without difficulty (*4*).

Figure 1(b) depicts a pair of plane surfaces sharing a common edge, which will be designated as the ad-

* Another important aspect of the standard theory is the postulate of diffuse reflection. A first step toward evaluating the effects of specular reflection has been taken in reference *5*.

joint plate system. The angle $\theta$ between the plates may be arbitrary. The radiation conditions for this system are the same as for the parallel plates of Figure 1(a), the upper surface 1 being black and the lower surface 2 having arbitrary emissivity. The third Figure 1(c) shows a pair of parallel co-axial disks of radius $R$ having radiation conditions of the same type as have been described for the previous figures. The disk system is made up of finite surfaces, whereas the other configurations considered have one dimension which is essentially infinite.

The coordinates for the three configurations pictured in Figure 1 are selected so as to permit a unified analysis for all. The coordinate $x$ measures distances along the lower (nonblack) surface, while $y$ measures distances along the upper (black) surface. In all cases the upper surface is denoted by 1 and has a temperature $T_1$, while the lower surface is denoted by 2 and has a temperature $T_2$.

## ANALYSIS

### Energy balances

The analysis is begun by writing radiant flux balances at typical positions on surfaces 1 and 2. In general for a nonblack surface the radiant energy $B$ (radiosity) leaving the surface consists of two parts: a direct emission and a reflection of the incident energy $H$. For a typical position $x$ on the lower (gray) surface 2

$$B_2(x) = \epsilon\sigma T_2^4 + \rho H_2(x) \qquad (1)$$

In almost all applications the incident energy $H$ will vary with $x$, and as a consequence the radiosity $B$ will vary even though $T_2$ is constant. It is the inclusion of this variation which marks the departure between the present analysis and the standard gray body enclosure theory. For the upper surface, where black body conditions prevail ($\epsilon = 1$, $\rho = 0$), the radiosity expression reduces to

$$B_1(y) = B_1 = \sigma T_1^4 \qquad (2)$$

Thus for the black surface the radiosity is uniform and equal to the emission.

Next the net local heat transfer per unit area $q$ leaving a surface element may be related to the incident energy. Noting that the net heat transfer is expressible as a difference being the outgoing and incoming energy, one may write

$$q = B - H \qquad (3)$$

For the nonblack surface the expression for $q$ may be rephrased with the radiation flux balance (1); thus

$$q_2(x) = \epsilon\sigma T_2^4 - \epsilon H_2(x) \qquad (4)$$

where $\rho = \alpha$ and $\alpha = \epsilon$. Additionally

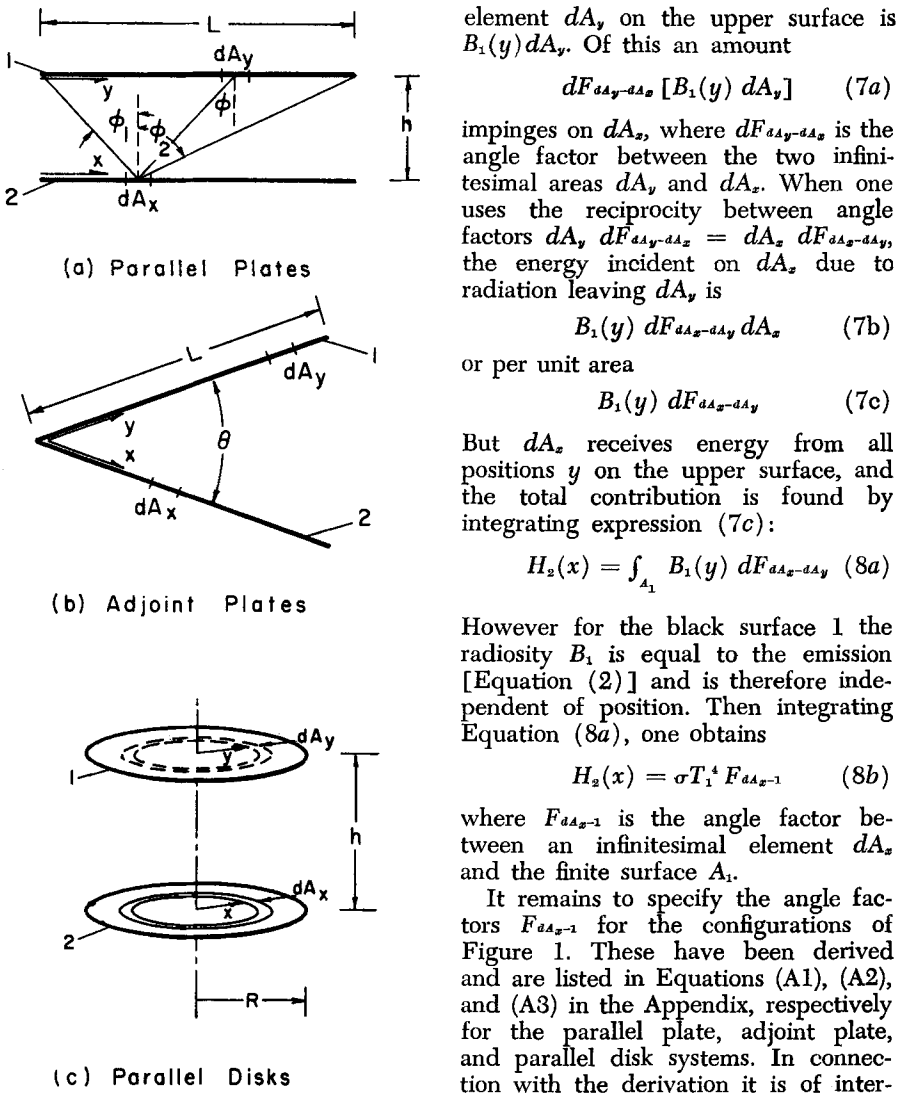


Fig. 1. Schematic of radiation systems.

for the black surface the combination of Equations (2) and (3) gives

$$q_1(y) = \sigma T_1^4 - H_1(y) \qquad (5)$$

So the distribution of the local heat transfer is immediately available as soon as the distribution of the incident energy is known. Further, from the local heat flux, the over-all net heat transfer $Q$ from a surface can be found by integrating; that is

$$Q = \int_A q\, dA \qquad (6)$$

### Incident energy flux on gray surface

Now one proceeds with the determination of the incident energy distributions $H_1(y)$ and $H_2(x)$. Consideration will first be given to $H_2(x)$, since it is easier to calculate and is also a necessary prerequisite for finding $H_1(y)$. Focusing attention on a typical area element $dA_x$ in Figures 1(a), (b), and (c), one may observe that the energy incident on such an element must be related to the radiation which leaves the upper surface 1. The radiant energy leaving in all directions from a typical element $dA_y$ on the upper surface is $B_1(y)dA_y$. Of this an amount

$$dF_{dA_y-dA_x}\,[B_1(y)\,dA_y] \qquad (7a)$$

impinges on $dA_x$, where $dF_{dA_y-dA_x}$ is the angle factor between the two infinitesimal areas $dA_y$ and $dA_x$. When one uses the reciprocity between angle factors $dA_y\, dF_{dA_y-dA_x} = dA_x\, dF_{dA_x-dA_y}$, the energy incident on $dA_x$ due to radiation leaving $dA_y$ is

$$B_1(y)\, dF_{dA_x-dA_y}\, dA_x \qquad (7b)$$

or per unit area

$$B_1(y)\, dF_{dA_x-dA_y} \qquad (7c)$$

But $dA_x$ receives energy from all positions $y$ on the upper surface, and the total contribution is found by integrating expression (7c):

$$H_2(x) = \int_{A_1} B_1(y)\, dF_{dA_x-dA_y} \qquad (8a)$$

However for the black surface 1 the radiosity $B_1$ is equal to the emission [Equation (2)] and is therefore independent of position. Then integrating Equation (8a), one obtains

$$H_2(x) = \sigma T_1^4 F_{dA_x-1} \qquad (8b)$$

where $F_{dA_x-1}$ is the angle factor between an infinitesimal element $dA_x$ and the finite surface $A_1$.

It remains to specify the angle factors $F_{dA_x-1}$ for the configurations of Figure 1. These have been derived and are listed in Equations (A1), (A2), and (A3) in the Appendix, respectively for the parallel plate, adjoint plate, and parallel disk systems. In connection with the derivation it is of interest to note a useful characteristic of systems such as 1(a) and 1(b) which consist of surfaces which are essentially infinite normal to the page, namely that the general expression for $F_{dA_x-1}$ has the remarkably simple form [reference 6, Equation (31-58)]:

$$F_{dA_x-1} = \frac{1}{2}(\sin\phi_1 + \sin\phi_2) \qquad (9a)$$

The angles $\phi_1$ and $\phi_2$ are illustrated in Figure 1(a) and are determined by the normal to $dA_x$ and the connecting lines between $dA_x$ and the extremities of surface 1.

As an abbreviation there is introduced the subscripted symbol $J$ to denote $F_{dA_x-1}$ for the systems under consideration. Thus
parallel plates:

$$F_{dA_x-1} \equiv J_\gamma,\ \gamma = h/L \qquad (10a)$$

adjoint plates:

$$F_{dA_x-1} \equiv J_\theta \qquad (10b)$$

parallel disks:

$$F_{dA_x-1} \equiv J_\nu,\ \nu = h/R \qquad (10c)$$

The angle factors as represented by the $J$ functions have been plotted as a

function of position $x$ on Figures 2, 3, and 4 respectively for the parallel plate, adjoint plate, and parallel disk systems. Parametric values of $\gamma$, $\theta$, and $\nu$ were selected to cover the range from openly-spaced to closely-spaced configurations. There are several trends which are evident from the figures. First, as the spacing becomes more open (larger $\gamma$, $\theta$, and $\nu$), the general level of the angle factor decreases (decreased interaction), but the distribution of the angle factor over the surface becomes more uniform. Next, for any given spacing the angle factor achieves its highest value at the most interior location in the system, for example at $x = L/2$ for the parallel plates and $x = 0$ for the parallel disks. In accordance with Equation (8*b*) the energy incident at $x$ is proportional to $F_{dA_x-1}$, and so the trends enumerated above apply directly to the incident energy. With the angle factors now determined the incident energy distribution on the lower surface $H_2(x)$ is also known, and this will be utilized later in the calculation of local heat transfer.

For the computation of the over-all net heat transfer from the entire lower surface it will be useful to have the total energy incident on that surface. This may be obtained by integrating Equation (8*b*); thus

$$\int_{A_2} H_2 dA = \sigma T_1^4 \int_{A_2} F_{dA_x-1}\, dA = \sigma T_1^4 A_2 F_{2-1} \quad (11)$$

where

$$F_{2-1} = \frac{1}{A_2}\int_{A_2} F_{dA_x-1}\, dA = \frac{1}{A_2}\int_{A_2} J\, dA \quad (11a)$$

The angle factor $F_{2-1}$ corresponds to radiant interchange between a pair of finite surfaces. The integration indicated in Equation (11*a*) is carried out in the Appendix, and the results are given in Equations (A4), (A5), and (A6). Numerical values of $F_{1-2} = F_{2-1}$ are listed in Table 1 for the same spacing parameters as were considered in Figures 2, 3, and 4. Inspection of the table indicates the expected trend that the angle factors increase as the spacing becomes closer.

This completes the incident energy calculation for the lower surface, and attention may now be directed to the corresponding calculation for the upper surface.

#### Incident energy on black surface

A portion of the analysis given above can be applied to the determination of $H_1(y)$; in fact Equation (8*a*) may be utilized provided that an interchange is made between 1 and 2 and also between $x$ and $y$; thus

Table 1. Angle Factors and Integrals

(a) Parallel plates

| $\gamma$ | $F_{1-2}$ | $F^2_{1-2}$ | $\frac{1}{L}\int_0^L I\, dy$ |
|---|---|---|---|
| 1 | 0.4142 | 0.1716 | 0.1724 |
| 0.5 | 0.6180 | 0.3820 | 0.3881 |
| 0.1 | 0.9050 | 0.8190 | 0.8317 |
| 0.05 | 0.9512 | 0.9049 | 0.9133 |

(b) Adjoint plates

| $\theta$ | $F_{1-2}$ | $F^2_{1-2}$ | $\frac{1}{L}\int_0^L I\, dy$ |
|---|---|---|---|
| 135° | 0.07612 | 0.00579 | 0.00670 |
| 90° | 0.2929 | 0.08578 | 0.09654 |
| 45° | 0.6173 | 0.3811 | 0.4091 |
| 30° | 0.7412 | 0.5493 | 0.5776 |

(c) Parallel disks

| $\nu$ | $F_{1-2}$ | $F^2_{1-2}$ | $\frac{1}{\pi R^2}\int_0^R I\, 2\pi r dr$ |
|---|---|---|---|
| 1 | 0.3820 | 0.1459 | 0.1501 |
| 0.5 | 0.6096 | 0.3716 | 0.3875 |
| 0.1 | 0.9049 | 0.8188 | 0.8338 |
| 0.05 | 0.9512 | 0.9048 | 0.9138 |

$$H_1(y) = \int_{A_2} B_2(x)\, dF_{dA_y-dA_x} \quad (12)$$

The radiosity $B_2(x)$ is taken from Equation (1) in conjunction with (8*b*), and with this $H_1(y)$ becomes

$$H_1(y) = \epsilon\sigma T_2^4 \int_{A_2} dF_{dA_y-dA_x} + (1-\epsilon)\sigma T_1^4 \int_{A_2} F_{dA_x-1}\, dF_{dA_y-dA_x} \quad (13)$$

The first integral can be immediately carried out to give

$$\int_{A_2} dF_{dA_y-dA_x} = F_{dA_y-2} = J \quad (14)$$

The angle factor $F_{dA_y-2}$ is available from Equations (A1), (A2), and (A3). Additionally the $J$ function plots of Figures 2, 3, and 4 also apply to $F_{dA_y-2}$.

To proceed with the second integral in Equation (13) it is necessary to know the two angle factors which appear under the integral sign. The first of these, $dF_{dA_x-1}$, has already been derived and is given as Equations (A1), (A2), and (A3) in the Appendix. The derivation of $dF_{dA_y-dA_x}$ is also carried out in the Appendix, and the results for the parallel plate, adjoint plate, and parallel disk configurations are embodied in equations (A7), (A8), and (A9) respectively. In connection with this latter derivation the parallel plate and adjoint plate configurations are especially tractable, since for any system having surfaces of essentially infinite extent normal to the page

$$dF_{dA_y-dA_x} = \frac{1}{2}\frac{d(\sin\phi)}{dx}dx \quad (9b)$$

The angle $\phi$, illustrated in Figure 1(a), is formed by the normal to $dA_y$ and the connecting line between $dA_y$ and $dA_x$.

With the angle factor expressions just discussed the second integral of Equation (13) may be evaluated. The integration is extended over the range $x = 0$ to $x = L$ for the parallel or adjoint plates and from $x = 0$ to $x = R$ for the parallel disks. After some study it was found that the integration could not be carried out analytically. Therefore numerical means were utilized. Introducing the abbreviation

$$I \equiv \int_{A_2} F_{dA_x-1}\, dF_{dA_y-dA_x} \quad (15)$$

one may plot the results of the numerical integration as solid lines on Figures 2, 3, and 4 respectively for the parallel plate, adjoint plate, and parallel disk configurations. These curves show trends similar to those previously discussed for the angle factor $J = F_{dA_x-1}$. But any $I$ curve always lies lower than the corresponding $J$ curve. This finding is easily understood when it is remembered that $J$ represents an angle factor for energy which crosses the gap but once, while $I$ corresponds to two crossings (back and forth).

Then one can return to Equation (13) for the incident energy and introduce the angle factor abbreviations of Equations (14) and (15), giving

$$H_1(y) = \epsilon\sigma T_2^4 J + (1-\epsilon)\sigma T_1^4 I \quad (16)$$

The distribution of $H_1$ as a function of $y$ can be calculated from Equation (16) for any set of temperature and emissivity values. The $I$ and $J$ functions needed in the computation may be read from Figures 2, 3, and 4.

In the over-all heat transfer computation for surface 1 it will be necessary to have the energy flux which is incident on the surface as a whole. Integrating Equation (16), one obtains

$$\int_{A_1} H_1(y)\, dA = \epsilon\sigma T_2^4 A_1 F_{1-2} + (1-\epsilon)\sigma T_1^4 \int_{A_1} I\, dA \quad (17)$$

In the first term on the right the angle factor $F_{1-2}$ is numerically equal to $F_{2-1}$ ($A_2 = A_1$). So Equations (A4), (A5), and (A6) can be applied directly, as can the numerical values in Table 1. The integral appearing in the last term, when combined with the definition of $I$ from Equation (15), leads to a double integration over $A_1$ and $A_2$. For the adjoint plate and parallel disk systems the double integral can be carried out in closed form giving the results respectively indicated in Equa-

tions (A10) and (A11). In the case of the parallel plates it was necessary to do the integration numerically. Table 1 lists numerical results for $\int I\,dA$ for all three configurations. Thus, when one utilizes the table, all terms in Equation (17) can be evaluated.

With complete information on the incident energy now at hand consideration can be given to the heat transfer calculation.

## LOCAL HEAT TRANSFER RESULTS

### Results for gray surface

The net local heat transfer per unit area from the gray surface 2 is obtained by introducing the incident energy (8*b*) into Equation (4):

$$\frac{q_2(x)}{\epsilon\sigma T_2^4} = 1 - \left(\frac{T_1}{T_2}\right)^4 F_{dA_{x-1}} \quad (18)$$

The equation indicates that $q$ is directly proportional to the emissivity $\epsilon$, and this is related to the fact that the incident energy is black. The variation of $q$ along the surface is due to the variation in angle factor. Now when one considers any one of Figures 2, 3, and 4, it is clear that the closer the spacing (smaller $\gamma$, $\theta$, or $\nu$) the greater will be the variation of $q$ over the surface. To obtain an easy appraisal of the extent of the variation, suppose for the moment that $T_1/T_2 = 1$. Then the heat transfer is proportional to $1 - F_{dA_{x-1}}$ or, in terms of Figures 2, 3, 4, to $1 - J$. But $1 - J$ is the distance between a $J$ curve and the top of the graph. Considering for instance Figure 2 one sees that at small spacings there can be an enormous variation of $q$ along the surface.

Further study of Equation (18) suggests that at any given spacing the variation of $q$ will be accentuated when the last term on the right is accentuated. This clearly will be the case when $T_1$ is large compared with $T_2$, or, in physical terms, when there is a large incident energy. Additionally the heat transfer may either be positive or negative (from or to the surface) depending upon the balance of incident and emitted energy. The interesting feature of this is that there may be a net loss ($q$ positive) on one portion of the surface, while another portion may be experiencing a net gain ($q$ negative).

These observations are graphically illustrated in Figure 5 for the parallel plate system with $\gamma = 0.5$, a fairly open spacing. The variation of $q$ is seen to increase as $T_1/T_2$ increases. For small $T_1/T_2$ (black surface relatively cold) the heat transfer is away from the surface 2 at all locations; the opposite is true at large $T_1/T_2$. For $(T_1/T_2)^4 = 2$ there is a heat loss near the edge of the plate (near $x = 0$) and a heat gain in the central region. A large number of graphs such as Figure 5 could be constructed corresponding to the various configurations and spacing parameters. Among these graphs there would be interesting differences in detail. For instance for close spacings (small $\gamma$, $\theta$, and $\nu$) the variations of the heat loss over the surface would be much more marked. However the general trends would not be different, and for this reason Figure 5 will suffice.

It might be well to mention that surface variations of the type discussed above cannot be calculated by the standard gray body enclosure theory. Instead only the over-all heat transfer can be computed. This is a noteworthy deficiency of the standard theory.

### Results for black surface

The distribution of the net local heat transfer for the black surface is found by introducing the incident energy expression (16) into Equation (5), giving

$$\frac{q_1(y)}{\sigma T_1^4} = 1 - (1-\epsilon)\,I - \epsilon\left(\frac{T_2}{T_1}\right)^4 J \quad (19)$$

where $I$ and $J$ denote angle factors which are plotted on Figures 2, 3, and 4. By inspection of Equation (19) it is clear that the dependence of the heat loss $q_1$ upon the emissivity $\epsilon$ of the gray surface is not a simple one. The two contributions to the incident radiant flux, the reflection of the black surface's own energy back upon itself and the emission of the gray surface, behave oppositely as $\epsilon$ changes. The magnitudes of these contributions also depend separately upon the spacing between the surfaces and the temperature ratio $T_2/T_1$.

Clearly when the gray surface is at a relatively low temperature ($T_2 << T_1$) and its emissivity is low, then the reflected energy will be the dominant factor in determining $q_1$. At the other extreme when the gray surface 2 is at a relatively high temperature ($T_2 >> T_1$) and has a high emissivity, then its emission is the dominating factor in fixing $q_1$. However when $T_2 > T_1$ and $\epsilon$ is low, or when $T_2 < T_1$ and $\epsilon$ is high, or when the temperatures are only moderately different and $\epsilon$ is moderate, then both terms may make important contributions.

The surface variation of $q_1$ is coupled with that of the angle factors $J$ and $I$, which are respectively associated with radiation travelling once or twice across the gap. As already noted these variations become more extreme as the spacing becomes closer. Additionally from Equation (19) it is seen that the surface variations in $q$ will be larger for larger values of $T_2/T_1$ at a fixed $\epsilon$. However it is by no means definite whether increasing $\epsilon$ will in-

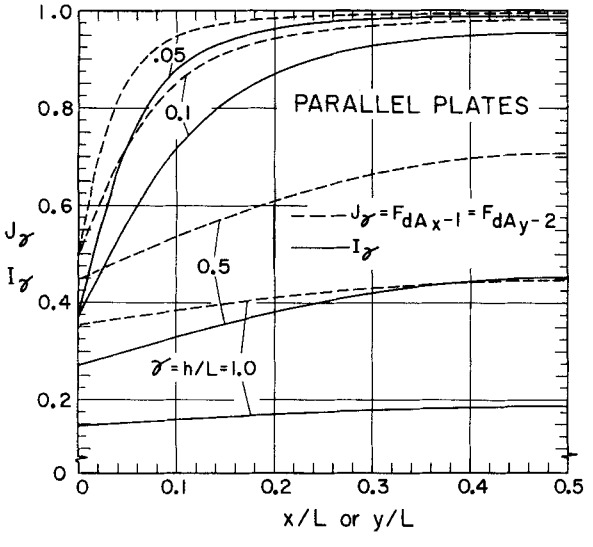


Fig. 2. Angle factors for parallel plate system.

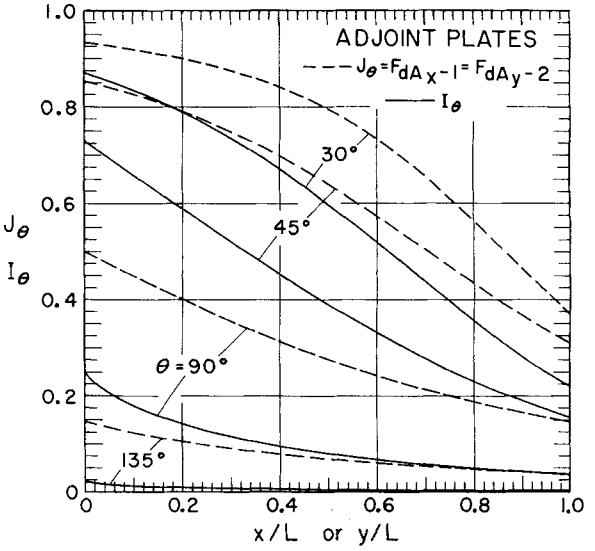


Fig. 3. Angle factors for adjoint plate system.

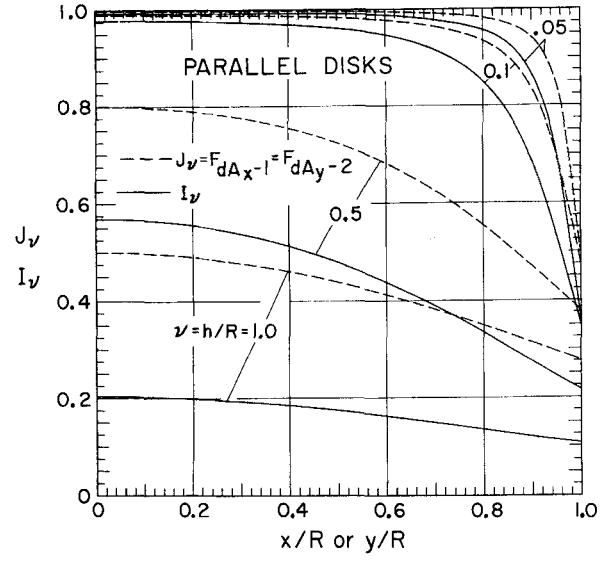


Fig. 4. Angle factors for parallel disk system.

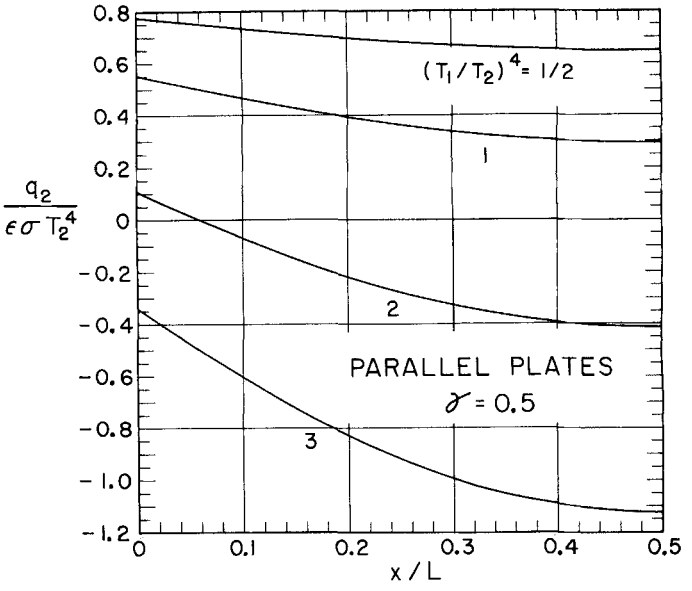


Fig. 5. Illustrative local heat transfer results for nonblack surface 2.

crease or decrease the surface variations in $q_1$; in fact either behavior is possible.

To illustrate the results which may be obtained by application of Equation (19) consideration has been once again given to the parallel plate case for the moderate spacing of $\gamma = h/L = 0.5$. Curves showing the distribution of $q_1$ along the surface are presented in Figure 6 for $\epsilon = 0.2$ and 0.9 for four values of the temperature ratio $T_2/T_1$. The effect of increasing $T_2/T_1$ (gray surface becoming relatively hotter) is to make the heat transfer distribution more nonuniform, and this effect is accentuated for larger values of $\epsilon$. Additionally the figure shows that $q_1$ may be either positive (heat loss) or negative (heat gain) depending on temperature and emissivity conditions.

As was the case for the gray surface the local heat transfer results for the black surface would also be unavailable from the standard enclosure theory.

## OVER-ALL HEAT TRANSFER RESULTS

The over-all heat transfer is perhaps the quantity of greatest technical interest. Of additional interest here are the possible comparisons between the present results for the over-all heat transfer and those of the standard enclosure theory. Now the behavior of a black surface should differ little from that of a highly-absorbent nonblack surface. Thus the comparison noted above should also provide a measure of the accuracy of the standard theory for interchange between two surfaces having different emissivities, one of which is high.

The net rate of heat transfer from a surface as a whole, $Q$, is found by integrating the local values in accordance with Equation (6). For the gray surface 2 integration of Equation (4) and subsequent substitution of the total incident flux from Equation (11) gives

$$\frac{Q_2}{\epsilon\sigma T_2^4 A_2} = 1 - \left(\frac{T_1}{T_2}\right)^4 F_{2-1} \quad (20)$$

The angle factor $F_{2-1}$ is given in the form of simple equations in the Appendix, and a listing for selected values of the spacing parameters is made in Table 1. For $T_1<T_2$ (black surface relatively cooler) the heat loss is positive (from the surface), since the angle factors are always less than unity. When $T_1$ is sufficiently large compared with $T_2$, $Q_2$ will become negative, and this will more readily occur for closer spacings because $F_{2-1}$ is larger.

For the black surface 1 integration of Equation (5) and substitution of Equation (17) yields

$$\frac{Q_1}{\sigma T_1^4 A_1} = 1 - (1-\epsilon)\frac{\int I dA}{A_1} - \epsilon\left(\frac{T_2}{T_1}\right)^4 F_{1-2} \quad (21)$$

To evaluate this equation $F_{1-2}$ and $(\int IdA)/A_1$ may be taken either from equations in the Appendix or from Table 1. Inspection of the table indicates that for open configurations the angle factor for back and forth travel $(\int IdA)/A$ will be substantially smaller than the angle factor for one way travel $F_{1-2}$. Additionally both angle factors are small compared with unity, and as a consequence the incident energy (last two terms on right) will play a minor role except when $T_2>>T_1$. On the other hand for close spacings both angle factors are large, and the incident energy plays a dominant role in determining the heat transfer. Further study of Equation (21) reveals that when $T_2<T_1$ (black surface hotter), there will always be a net heat loss from the surface $Q_1>0$. When $T_2>T_1$ (gray surface hotter), there may be either a heat gain or heat loss, depending on the spacing, emissivity, and temperature. To illustrate this consider the parallel plate system with spacing $\gamma = h/L = 0.5$. For $\epsilon = 0.2$ and $(T_2/T_1)^4$ taking values of 1/3, 1, and 3 it is found that $Q_1/\sigma T_1^4 A_1 = 0.648$, 0.566, and 0.319. For these same temperature ratios, but with $\epsilon = 0.9$, the values of $Q_1/\sigma T_1^4 A_1$ are 0.776, 0.405, and −0.707. This illustration also shows that with increasing emissivity of the gray surface the heat loss $Q_1$ may either increase or decrease depending upon the temperature ratio.

Attention will now be directed to comparisons with the over-all heat transfer predictions of the standard enclosure theory. These latter results may be derived as follows. First when one considers the radiosities, it is assumed that $B_2(x) = B_2 =$ constant, and additionally $B_1 = \sigma T_1^4 =$ constant. Next when one notes that

$$H_1 = B_2 F_{1-2}, \quad H_2 = B_1 F_{2-1}$$

it follows from Equations (1) and (2) that

$$H_1 = \epsilon\sigma T_2^4 F_{1-2} + (1-\epsilon) H_2 F_{1-2} \quad (22a)$$

$$H_2 = \sigma T_1^4 F_{1-2} \quad (22b)$$

The incident energy distributions $H_1$ and $H_2$ are uniform over the surface, and this is a consequence of the assumed uniformity of the radiosity. From Equations (4), (5), and (6) it then follows that $q$ is uniform over the surface and equal to $Q/A$. When one utilizes $H_1$ and $H_2$ from above, the heat transfer evaluated from (4) and (5) is

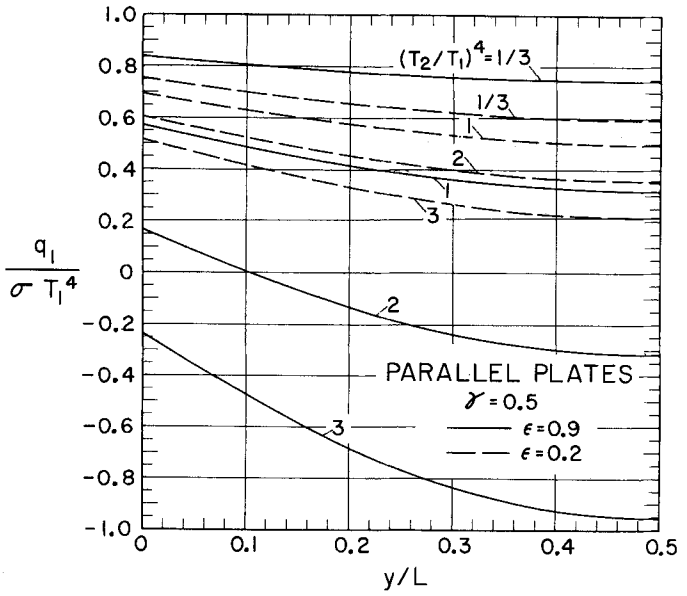


Fig. 6. Illustrative local heat transfer results for black surface 1.

$$\frac{Q_2^*}{\epsilon\sigma T_2^4 A_2} = 1 - \left(\frac{T_1}{T_2}\right)^4 F_{2\text{-}1} \quad (23)$$

$$\frac{Q_1^*}{\sigma T_1^4 A_1} = 1 - (1-\epsilon)\, F^2_{2\text{-}1} - \epsilon\left(\frac{T_2}{T_1}\right)^4 F_{2\text{-}1} \quad (24)$$

where the asterisks denote the standard enclosure theory.

Comparing the heat loss (23) with the previously derived result (20) for the nonblack surface 2 one sees that the two expressions are identical. This is to be expected, since the energy falling on 2 comes from a surface of uniform radiosity, the black, isothermal plate 1.

Next comparing Equations (24) and (21) for the black surface one sees that differences occur in the middle term on the right side. This term corresponds to the reflection of 1's own emission back upon itself, and the differences arise because Equation (21) takes account of the nonuniform distribution of the reflected energy leaving surface 2, while Equation (24) does not. The absolute error in the heat transfer prediction is found by differencing Equations (21) and (24); thus

$$\frac{Q_1^* - Q_1}{\sigma T_1^4 A_1} = (1-\epsilon)\left[\frac{\int I dA}{A_1} - F^2_{2\text{-}1}\right] \quad (25)$$

Referring to Table 1 one sees that the bracketed quantity on the right side of Equation (25) is always positive. When the heat transfer is from the surface ($Q_1>0$), $Q^*$ predicts too high a heat loss, while if the heat transfer is to the surface, $Q^*$ predicts too low a heat gain.

Equation (25) states that the absolute error is largest when surface 2 is highly reflecting (small $\epsilon$) and when the spacing is close (see Table 1). Further inspection of the equation and the table reveals that the absolute error will never be more than 1 or 2% of the emission $\sigma T_1^4 A$. However the error relative to the actual net heat transfer may be much larger. Utilizing Equations (25) and (21) one gets

$$\frac{Q_1^* - Q_1}{Q_1} = \frac{(1-\epsilon)\left[\frac{\int I dA}{A_1} - F^2_{2\text{-}1}\right]}{1-(1-\epsilon)\frac{\int I dA}{A_1} - \epsilon\left(\frac{T_2}{T_1}\right)^4 F_{2\text{-}1}} \quad (26)$$

The relative errors given by Equation (26) will continue to be acceptable for most applications as long as $|Q_1|$ is say $\geqslant 0.2\,\sigma T_1^4 A$ (a 5 or 10% relative error). But for $Q_1$ values smaller than this care must be taken. A criterion for delineating the danger region may be obtained by setting the denominator of Equation (26) equal to zero and replacing $\int I dA/A_1$ by $F^2_{2\text{-}1}$ for computational simplicity:

$$\frac{T_2}{T_1} \sim \left[\frac{1}{\epsilon F_{2\text{-}1}} - \frac{(1-\epsilon)}{\epsilon} F_{2\text{-}1}\right]^{1/4} \quad (27)$$

From this it appears that the danger region will usually be associated with $T_2/T_1 > 1$, with increasingly higher temperature ratios required as the spacing becomes more open.

From this discussion it might be expected that for $T_2 < T_1$ (gray surface relatively cool) the relative error will always be small, especially when $\epsilon$ is large and the spacing open. For $T_2 > T_1$ such a blanket assertion cannot be made.


## ACKNOWLEDGMENT

The support of this research by the National Science Foundation under grant G10177 is gratefully acknowledged. The author also wishes to acknowledge the contributions of Mr. G. G. Hingorani and Mr. K. Sreenivasan, in connection with the calculations.


## NOTATION

$A$ = surface area
$B$ = radiosity (radiant flux leaving surface per unit time and area)
$F$ = angle factor
$H$ = incident energy per unit time and area
$h$ = spacing between plates or disks
$I$ = abbreviation for angle factor integral, Equation (15)
$J$ = angle factor, $F_{dA_x\text{-}1}$ and $F_{dA_y\text{-}2}$
$L$ = plate length
$Q$ = over-all rate of heat loss
$q$ = local rate of heat loss per unit area
$R$ = radius of disk
$T$ = absolute temperature
$X$ = dimensionless coordinate, $x/L$ or $x/R$
$x$ = coordinate on nonblack surface 2
$Y$ = dimensionless coordinate, $y/L$ or $y/R$
$y$ = coordinate on black surface 1

### Greek Letters

$\alpha$ = absorptivity
$\gamma$ = spacing ratio, $h/L$
$\theta$ = opening angle
$\epsilon$ = emissivity
$\nu$ = spacing ratio, $h/R$
$\rho$ = reflectivity, $1-\alpha$
$\sigma$ = Stefan-Boltzmann constant
$\phi_1,\phi_2,\phi$ = angles on Figure 1(a)

### Subscripts

1 = black surface
2 = nonblack surface
$x$ = local position on surface 2
$y$ = local position on surface 1

## LITERATURE CITED


1. McAdams, W. H., "Heat Transmission," 3 ed., Chap. 4, McGraw-Hill, New York (1954).
2. Eckert, E. R. G., and R. M. Drake, Jr., "Heat and Mass Transfer," McGraw-Hill, New York (1959).
3. Sparrow, E. M., J. L. Gregg, J. V. Szel, and P. Manos, *J. Heat Transfer*, 83C, 207-214 (1961).
4. Sparrow, E. M., and J. L. Gregg, *ibid.*, to be published.
5. Eckert, E. R. G., and E. M. Sparrow, *Intern. J. Heat and Mass Transfer*, 3, 42-54 (1961).
6. Jakob, Max, "Heat Transfer," Vol. 2, Wiley, New York (1957).



*Manuscript received February 1, 1961; revision received July 7, 1961; paper accepted July 10, 1961.*

## APPENDIX

### Angle Factors

When one considers first the angle factor $F_{dA_{g-1}}$, the general expression (9*a*) for surfaces having one infinitely elongated dimension can be applied to the parallel plate and adjoint plate systems of Figures 1(a) and 1(b), respectively, yielding

$$F_{dA_{g-1}} = \frac{1}{2}\left\{\frac{1-X}{\sqrt{(1-X)^2+\gamma^2}} + \frac{X}{\sqrt{X^2+\gamma^2}}\right\} \quad (A1)$$

$$F_{dA_{g-1}} = \frac{1}{2}\left\{1 + \frac{\cos\theta - X}{\sqrt{1-2X\cos\theta+X^2}}\right\} \quad (A2)$$

For the parallel disk system the derivation is carried out with angle factor algebra as in Equations (33) and (34) of reference 4, with the result

$$F_{dA_{g-1}} = \frac{1}{2}\left\{1 - \frac{\nu^2 - 1 + X^2}{\sqrt{[\nu^2+1+X^2]^2 - 4X^2}}\right\} \quad (A3)$$

The angle factor $F_{2-1}$ for interchange between two finite surfaces is obtained by direct integration in accordance with Equation (11*a*). The end results for the parallel plate, adjoint plate, and parallel disks system are respectively as follows:

$$F_{2-1} = \sqrt{1+\gamma^2} - \gamma \quad (A4)$$

$$F_{2-1} = 1 - \sin(\theta/2) \quad (A5)$$

$$F_{2-1} = \frac{1}{2}\{2 + \nu^2 - \nu\sqrt{\nu^2+4}\} \quad (A6)$$

Next when one considers the infinitesimal angle factor $dF_{dA_y-dA_x}$, application of Equation (9*b*) to the parallel plate and adjoint plate systems yields

$$dF_{dA_y-dA_x} = \frac{\gamma^2}{2}\frac{dX}{[(X-Y)^2+\gamma^2]^{3/2}} \quad (A7)$$

$$dF_{dA_y-dA_x} = \frac{1}{2}\frac{XY(1-\cos^2\theta)\,dX}{[X^2+Y^2-2XY\cos\theta]^{3/2}} \quad (A8)$$

The corresponding result for the parallel disks is taken directly from Equation (36) of reference 4:

$$dF_{dA_y-dA_x} = 2\nu^2\frac{(\nu^2+X^2+Y^2)\,X\,dX}{[(\nu^2+X^2+Y^2)^2-4X^2Y^2]^{3/2}} \quad (A9)$$

Finally the double integral appearing in the last term of Equation (17) may be carried out in closed form for the adjoint plate and parallel disk systems. The respective results of the integration are

$$\frac{1}{L}\int_o^L IdA = 1 - \sin(\theta/2) + \frac{1}{8}(\theta-\pi)\sin\theta \quad (A10)$$

$$\frac{1}{\pi R^2}\int_o^R IdA = \frac{1}{2}\left\{2 + \nu^2 - \nu\sqrt{\nu^2+4} - \nu\tan^{-1}\frac{\nu}{2} + \nu\tan\left(\frac{\nu}{2} - \frac{1}{2\nu}\right)\right\} \quad (A11)$$

The corresponding integration for the parallel plate system could not be carried out in closed form.

---

# Prediction of Pressure Drop in Two-Phase Single-Component Fluid Flow

**M. R. HATCH and R. B. JACOBS**

**National Bureau of Standards, Boulder, Colorado**

**Data on pressure drop in two-phase, single-component fluid flow, both with and without heat transfer, are presented in terms of the Lockhart and Martinelli correlation parameters. The fluids used were trichloromonofluoromethane and hydrogen.**

**The results are compared with the correlation curve recommended by Martinelli and Nelson and give frictional pressure drops that are about 40% lower than the curve. The reasons for the deviations are discussed in terms of the effects of friction factors, the existence of metastable equilibrium, accuracy of data and instrumentation, and calculation procedures.**

**It is concluded that the Martinelli and Nelson correlation and a simple momentum pressure drop computation can be superposed to predict roughly the total pressure drop in tubes containing steady state, two-phase, single-component fluid flow with appreciable vaporization.**

The fluid mechanical design of piping systems is handicapped by lack of information concerning so-called *steady state*, two-phase, single-component fluid flows. The objective of the investigation described here was to provide some of the required information. Data have been obtained and correlated for two-phase, single-component fluid flows, both with and without heat transfer. The results of some experiments with liquid hydrogen flowing with large heat flux (*11*), as well as those obtained from an extensive investigation with trichloromonofluoromethane, are reported. For the latter investigation the quality was varied from zero to unity; the Reynolds number based upon the total mass flow being saturated liquid (that is zero quality), was varied from about 5,000 to 90,000; the pressure and temperature were varied so that fluid properties changed significantly; and the diameter of the test section was varied. In addition single-phase (liquid) friction factors, which differ appreciably from published data (*10*), were determined.

Because the mathematical models required for theoretical analysis of two-phase flow problems are complex, the more successful approaches have been empirical and semiempirical. The majority of theoretical analyses, for example Harvey and Foust (*3*), have assumed that the fluid is homogeneous. The work of Linning (*7*) is an example of a semiempirical approach; Linning set up one-dimensional models for both stratified and annular flow configurations, determining unknown parameters experimentally. Lockhart and Martinelli (*8*) present a moderately successful correlation for the two-component problem.

Rogers (*12*) utilized the equations of Harvey and Foust to predict the